Comparing transient oligonucleotide hybridization kinetics using DNA-PAINT and optoplasmonic single-molecule sensing on gold nanorods

Narima Eerqing [1,2,*], Sivaraman Subramanian [1,2], Jesús Rubio [2], Tobias Lutz [1,2], Hsin-Yu Wu [1,2], Janet Anders [2,3], Christian Soeller [1,2], and Frank Vollmer [1,2]

1 Living Systems Institute, University of Exeter, Stocker Road, Exeter, EX4 4QD, United Kingdom

2 Department of Physics and Astronomy, University of Exeter, Stocker Road, Exeter EX4 4QL, United Kingdom

3 Institut für Physik und Astronomie, University of Potsdam, 14476 Potsdam, Germany

Keywords: *single-molecule kinetics; DNA hybridization; DNA-PAINT; optoplasmonic sensing; whispering gallery mode sensor.*

ABSTRACT: We report a comparison of two photonic techniques for single-molecule sensing: fluorescence nanoscopy and optoplasmonic sensing. As the test system, oligonucleotides with and without fluorescent labels are transiently hybridized to complementary 'docking' strands attached to gold nanorods. The measured single-molecule kinetics is compared to discern the influence of fluorescent labels as well as factors arising from different sensing geometries. Our results demonstrate that DNA dissociation is not significantly altered by the fluorescent label, while DNA association is affected by geometric factors in the two techniques. These findings open the door to exploiting plasmonic sensing and fluorescence nanoscopy in a complementary fashion, which will aid in building more powerful sensors and uncovering the intricate effects that influence the behavior of single molecules.

Biomolecules inhabit a microbiological environment sufficiently complex for their state to vary such that biological processes operate far from thermodynamic equilibrium. As a result, information extracted with ensemble measurements can be insufficient to predict the behavior of biomolecules, since ensemble averages may be far from the state of any single molecule in the system.[1, 2] The alternative is to probe biomolecular activity directly by using single-molecule techniques,[3-6] which do not only provide mean values of physical observables but also more detailed statistics in the form of probability distributions. A plethora of photonics-based techniques for single-molecule detection has emerged in the past decade. For example, single-molecule localization microscopy (SMLM)[7-9] has overcome the diffraction limit, enabling the reconstruction of images with great precision via temporal modulation and the accumulation of single-molecule detection events. Examples include photo-activated localization microscopy (PALM),[8] stochastic optical reconstruction microscopy (STORM),[7] and DNA-based point accumulation for imaging in nanoscale topography (DNA-PAINT).[10-12] On the other hand, single-molecule detection that makes use of noble-metal nanostructures has attracted great attention owing to the exceptional sensitivity arising from localized surface plasmon resonance (LSPR).[13, 14] The local enhancements of optical near-fields around gold nanorods (GNRs) have enabled particularly high detection sensitivities for biomolecules without the need for fluorescent labels.[15-17] Among the family of LSPR-based techniques, the combination of whispering-gallery-mode (WGM) sensing with plasmonic nanorods (optoplasmonic sensing) has shown a very high detection sensitivity even down to small biomolecules such as short DNA oligonucleotides.[18-20]

Despite this steady progress, single-molecule techniques suffer from different drawbacks that limit the information one can extract. For example, it is well-known that fluorescent labels may affect the kinetics and dynamics of biomolecular systems,[21-23] while LSPR-based approaches use local field enhancements that are not uniform across a plasmonic nanostructure, and the local surface geometry and heterogeneity of plasmonic nanoparticles can play a significant role in the observed statistics.[24-26] In view of this, finding an accurate description of bioprocesses at the single-molecule level will require the combination of information arising from different methods applied to the same molecular system. But, to guarantee the validity of such an approach, current single-molecule techniques must be compared and cross-validated.

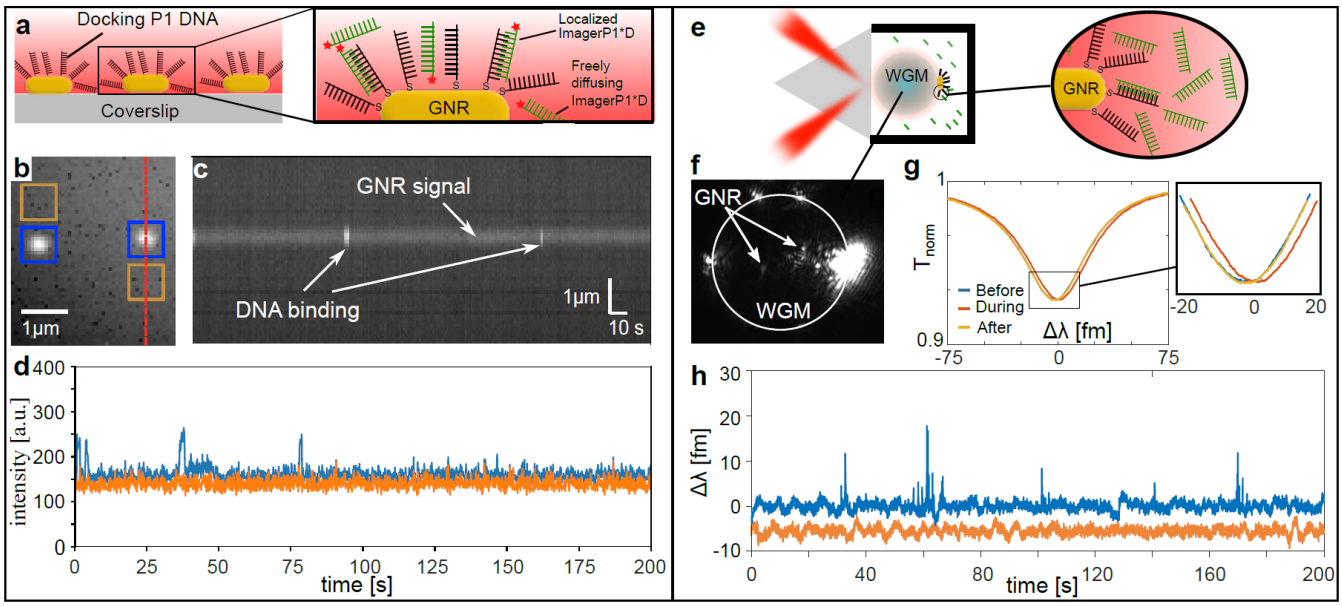


Figure 1. Comparison between DNA-PAINT (a-d) and WGM (e-h) methods. (a) Schematic of DNA-PAINT experiment on gold nanorods (GNRs). GNRs with LSPR ~780 nm (yellow) are coated with DNA docking strands P1 (black) and immobilized on the surface of a coverslip (grey). The zoomed view shows a single immobilized GNR. P1*D imager strands (green) functionalized with ATTO 655 (red star) are added and excited. (b) Microscope image showing the signal from the GNRs (blue box) and adjacent from GNR (orange box) positions. (c) A space-time plot of the red line through one GNR in (b). The GNRs provide a constant intensity over time and the hybridization of the imager ssDNA is observed as short bursts of increased intensity. (d) Typical fluorescence time traces, with orange and blue lines showing the intensity signal at the locations indicated in (b). (e) Schematic of WGM sensing approach. A laser beam is focused on the surface of the prism and coupled into a glass microsphere. GNRs are then immobilized on the surface of the microsphere. The zoom-in shows docking strands P1 (black) immobilized on the GNRs surface and imager strands P1* diffusing freely in solution. (f) Microscope image of the glass microsphere with GNRs immobilized on its surface. The scattering from the GNRs is observed as bright spots. (g) An example of wavelength shift caused by the hybridization of the imager and docking strands on the sensor. The blue, orange, and yellow curves represent the WGM mode position before, during, and after a single molecule transient event. (h) Typical detrended time trace of WGM resonance wavelength showing background signal (orange) and signals obtained for DNA hybridization (blue). All experiments were conducted at room temperature (22.5 °C).

Here we compare the detection of DNA hybridization using two established photonic single-molecule techniques: DNA-PAINT and WGM-based optoplasmonic sensing (see schematic in Figure 1). We employ a 13-mer single-stranded DNA (ssDNA), termed P1, and the complementary labeled (with Atto655) and unlabeled imager strands, named imager P1*D and imager P1*, respectively (see Table 1). In both techniques, the P1 strands are attached to gold nanorods via covalent thiol bonds and serve as the docking strands, while the imager strands are freely diffusing in solution. The oligonucleotide sequence is chosen to allow for transient hybridization events at room temperature. This arrangement allows us to test the impact of (i) the presence of labels, and (ii) the potential influence of the gold nanorod surface. Specifically, DNA-PAINT labels the imager strands with dye molecules and collects signals from docking strands attached anywhere on the GNRs surface, while the optoplasmonic technique is label-free and acquires signals predominantly from the tips of the GNRs.[19]

Our measurements reveal that the dissociation rates of hybridized DNA strands are approximately the same for both techniques. Thus, the modification of a 10-mer oligonucleotide with an Atto655 dye at its 5' end does not significantly affect the hybridization kinetics. On the other hand, the rates of association of the complementary strands as measured by the two techniques differ by ~3 orders in magnitude. This discrepancy likely originates from differences in the surface heterogeneities of the gold nanorods, as well as in the fraction of strands that are contributing to the signals in the two experimental techniques.

Table 1. Sequences of ssDNA used for the experiments.

ssDNA	Sequence (5' – 3')
P1	[ThiolC6] TTT TAT ACA TCT A
imager P1*D	[Atto655] CTA GAT GTA T
imager P1*	CTA GAT GTA T

The layout of the DNA-PAINT experiment is shown in Figure 1a. The protocol is adapted from Taylor et al.[27] First, Gold nanorods (A12-10-CTAB-750; Nanopartz Inc.) are

functionalised with the 13mer docking strand P1 via the mercaptohexyl linker (on 5' end), a procedure that is conducted in a pH ~ 3 citrate buffer with 1 M of NaCl. In particular, we add 1 μM of docking strands, and we leave them in the chamber over 30 min. On average, the diameter of GNRs is 10 nm, while their length is 35 nm. Furthermore, they exhibit a longitudinal surface plasmon resonance of 780 nm, which is far detuned from the laser wavelength (647nm). Hence, we do not expect any significant quenching or enhancement of fluorescence by the plasmonic effects. Following the pre-attaching of docking strands onto GNRs, a clean coverslip is functionalized with PLL-g-PEG (SuSos), whose role here is to prevent unspecific binding between fluorophore and the coverslip. GNRs are then permanently adsorbed onto the surface of the coverslip within an acidic dilute aqueous suspension (pH=1.6, 0.1nM). The experiment is carried out on a Nikon Ti-E inverted microscope with a 1.49 NA total internal reflection fluorescence (TIRF) objective (Nikon Apo TIRF 60X oil) illuminated using a 647 nm laser (OMicron LuxX 647- 140) and custom-built optics. The GNRs are excited via TIR at the coverslip and their photoluminescence is visualized real-time by the sCMOS camera (Andor Zyla 4.2 USB 3.0) as they bind to the glass coverslip (see Figure 1b). The experiment is run over for 15 min for the GNRs to freely deposit. The chamber is washed 3 times to remove unbound GNRs and changed the buffer to Tris-EDTA (TE buffer) with 500 mM of NaCl, where the latter provides the necessary ionic strength required for the desired DNA-binding kinetics. We then add into the chamber different concentrations of the imager P1*D modified with ATTO 655 (on the 5' end). Finally, the fluorescence signals from the hybridization of the DNA strands are recorded over time and co-localized with the position of the GNRs, as shown in Figure 1b (blue boxes). Figure 1c shows a space-time plot for the red line shown in Figure 1b. The constant intensity background indicates the GNR photoluminescence, and the burst of intensity indicates DNA hybridization between P1 and imager P1*D that co-localized with GNR position. Using this information, we plot a fluorescence time trace as shown in Figure 1d. The blue curve shows the DNA hybridization between P1 and imager P1*D, and the orange curve displays the background signal adjacent to the GNR position. Along this time trace, most of the signals we observe are spike-like, although it is also possible to detect plateau-like signals (see Figure 2a) indicating prolonged interactions between imager and docking strands. The frame rate is 100 ms/frame and experiments were conducted at 22.5 °C.

A scheme of the second single-molecule detection technique employed, i.e., an optoplasmonic sensor, is shown in Figure 1e. The input laser beam is focused on the surface of a prism and then coupled to a glass microsphere of diameter ~ 80 μm, generating an evanescent field around the microsphere. This field excites the surface plasmon resonance of several GNRs (12-20 on average) that are attached near the equator of the microsphere (see Figure 1f). The input laser wavelength is swept every 100 ms to record the transmission spectrum of narrow plasmon-coupled WGM, see Figure 1g. The sensing mechanism consists in recording wavelength shifts that are produced when a molecule enters the hotspots (i.e., the local field enhancements) of the GNRs. In practice, this involves tracking the changes in the WGM resonance position by fitting Lorentzian functions, from where we can obtain temporal traces for the wavelength shift Δλ. A trace example is shown in Figure 1h, where the blue curve shows spike signals that indicate single-molecule hybridization events, and the orange curve is the background signal when no imager P1* was added. To fabricate the sensor, a glass microsphere with a diameter of ~ 80 μm is melted at

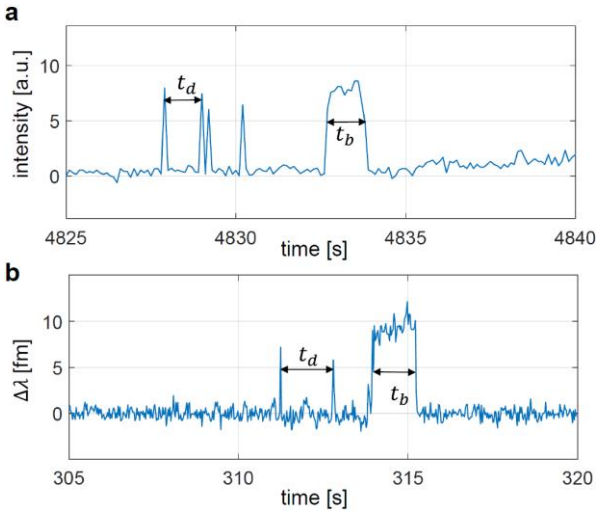


Figure 2. Examples of detailed traces generated by the interactions between docking and imager strands in (a) the DNA-PAINT experiment, and (b) the WGM sensing technique. Here t_b denotes the time that a strand spends in a bounded state, while t_d indicates the time between detected single-molecule hybridization events.

the end of an optical fiber using a high-power CO_2 laser and placed in the chamber. Next, the chamber is filled with 500 μl of ultra-pure water with pH adjusted to ~ 1.6 using 1M HCl. Then, approximately 1 pM of GNRs is added to the sample chamber. The GNRs, of the same type as described in the DNA-PAINT experiment, are then adsorbed onto the microsphere. A picture of the microsphere attached with GNRs is shown in Figure 1f. The docking strands are then immobilized on the GNRs as described for the DNA-PAINT experiment, i.e., once the GNRs are deposited, we wash the chamber several times and add citrate buffer pH ~ 3 with 1M NaCl, after which we add 1 μM of thiolated docking strand, P1. This is then left for 30 mins. Next, we change the buffer to TE buffer (containing 500mM NaCl) and add the imager P1* (with no dye attached); during this process, several spike signals appear in the $\Delta\lambda$ trace. Additionally, we occasionally observe a small plateau-like signal, as shown in Figure 2b. The lower part of such signal corresponds to an un-

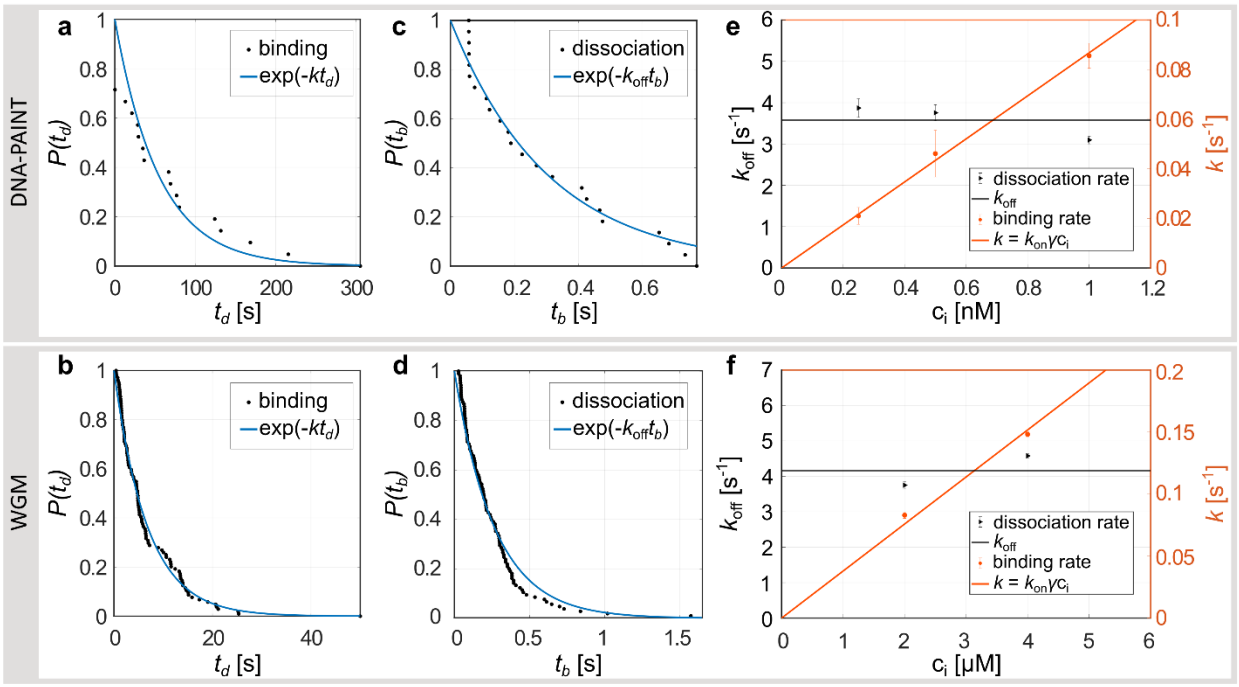


Figure 3. Shown are the probabilities P that a binding event has not taken place within an interval t_d for (a) DNA-PAINT and (b) WGM experiments, measured (black dots) and fit (blue line). Similarly, the probability that a dissociation event has not taken place within an interval t_b is shown in (c) (DNA-PAINT) and (d) (WGM). The single-molecule dissociation rate k_{off} (black) and the binding rate $k = k_{on}\gamma c_i$ (orange), both with units of s^{-1}, are shown for (e) DNA-PAINT and (f) WGM sensing, where k_{on} is the association rate constant with units of $M^{-1}s^{-1}$, γ is a numerical factor accounting for the geometric arrangement and accessibility of the docking strands contributing to the signals, and c_i is the molar imager concentration. Our results show that the dissociation rate for the DNA-PAINT and the optoplasmonic techniques are the same within error. For binding kinetics, only the product $k_{on}\gamma$ is retrieved.

occupied docking strand, while the spike-like signals indicate the transient hybridization of the docking strand P1 with an imager P1*. The laser sweep frequency is 50Hz, and the tracking of the resonance position occurs at the 20 ms time intervals. This experiment is also conducted at 22.5 °C.

DNA hybridization has previously been reported[28, 29] to follow (pseudo) first-order kinetics. Considering a single docking strand that can be found in two states, either bounded with a single imager strand or dissociated, the probability that a binding event does not take place in an interval t_d (dissociated waiting time), also called survival probability, is $P^s(t_d) = \exp(-k_s t_d)$ where k_s is a single-molecule binding rate with units of s^{-1} (also known as association rate). However, the traces of both experiments (Figure 2) record the signal of binding events triggered by many imager strands, and the chance of observing the binding of one of the imagers in the chamber is further affected by the arrangement and accessibility of docking strands contributing to the signals on each sensor. The probability distribution for the waiting time to detect the binding of any one of the imagers, assuming independence of events, is then $P(t_d) = \exp(-k\, t_d)$, where $k = k_{on}\gamma\, c_i$ is a rate with units of s^{-1}. Here, k_{on} is the usual on-rate constant per unit of concentration, γ is a numerical factor accounting for the geometric arrangement of the docking strands and their contribution to the observed signals, and c_i is the imager concentration. Since the factor γ is constant within the same experimental setup we expect that, for each experiment, the rate k grows linearly with c_i. Once a docking strand is bound, the probability that dissociation does not take place in an interval t_b (bound waiting time) is $P(t_b) \simeq \exp(-k_{\text{off}}\, t_b)$, where k_{off} is the dissociation rate constant and, in this case, equivalent to a single molecule dissociation rate with units of s^{-1}. In other words, we expect k_{off} to be concentration-independent[28, 29]. Note that the approximation holds provided that the chance of two imagers being bound at the same time is negligible, which is achieved by making the imager concentration sufficiently low.

Using the values for the two waiting times, t_d and t_b, all measured at temperature 22.5°C, we first computed the empirical distributions $P(t_d)$ and $P(t_b)$, both for the DNA-PAINT experiment (dotted line in Figure 3a,c) and the WGM platform (dotted line in Figure 3b,d). As expected, exponential profiles emerge, from which the rates k and k_{off} are extracted for different molar imager concentrations c_i. The product $k_{on}\gamma$ is further calculated by a linear fit yielding $k_{on}\gamma^{\text{PAINT}} = (8.7 \pm 0.3) \times 10^7\, M^{-1}s^{-1}$ and $k_{on}\gamma^{\text{WGM}} = (3.8 \pm 0.4) \times 10^4\, M^{-1}s^{-1}$ (estimate ± SE) for the DNA-PAINT and WGM experiments, respectively. These fits are shown in Figure 3e,f, and for DNA-PAINT we see clear evidence of a linear dependence between k and c_i. The value of

k_{on} cannot be determined without knowledge of the geometric factors. While the determination of γ for each technique lies beyond the scope of this work, we can highlight some factors contributing to its value. For instance, all docking strands contribute to the signal in DNA-PAINT, whereas only 12% of the docking strands in the WGM technique (attached to the tips of the GNRs) contribute to the signal. Additionally, the local surface properties will be different for the tips compared to the sides of the GNRs.[24-26]

More importantly, the single-molecule dissociation rate k_{off} can be directly obtained from the fits to $P(t_b)$ in Figure 3c (DNA-PAINT) and 3d (WGM). As expected, the k_{off} values are indeed approximately constant across all trials with different imager concentrations c_i, as can be seen in Figures 3e and 3f. The resulting dissociation rates are $k_{\text{off}}^{PAINT} = 3.6 \pm 0.4\ s^{-1}$ and $k_{\text{off}}^{WGM} = 4.2 \pm 0.8\ s^{-1}$ for DNA-PAINT and WGM, respectively. Thus the value of k_{off} measured by both techniques is the same within error, suggesting that the fluorescent dye molecule in P1*D does not significantly alter the kinetics for the DNA hybridization under study. Nevertheless, previous studies[30] have shown that kinetics of biomolecular systems can be influenced by the presence of fluorophores, and so the impact of fluorophores may have to be examined in a case-by-case basis. The compatible k_{off} values also show that there is no evidence of a local temperature increase due to the near-field enhancement of the GNRs at the light intensities used in both techniques.

Here we have compared two optical single-molecule detection techniques, fluorescence nanoscopy (DNA-PAINT) and optoplasmonic WGM sensing, that utilize the same plasmonic nanoparticles for detecting DNA hybridization events between surface immobilized docking strands and imager strands in solution. The rate constant k_{off}, which characterizes the dissociation of the DNA sequences used here, should depend only on the oligonucleotide sequence and length (buffer and temperature conditions are the same across experiments) while being independent of the different geometric factors of the two experiments. Indeed, we found k_{off} to be the same in both experiments, within experimental error. This establishes the equivalence of each technique for this test system and can serve as the basis for consistently combining these techniques in future single-molecule studies. In particular, to establish the dissociation rates for other processes, one may benefit from the larger binding efficiency of DNA-PAINT, while checking the label-impact with the WGM platform.

AUTHOR INFORMATION

Corresponding Author

*ne276@exeter.ac.uk

Author Contributions

N.E. and J.R. analyzed the data and wrote the manuscript.; S.S. carried out the WGM-based experiment; T.L. and SS conducted the DNA-PAINT experiments; T.L. and C.S. analyzed the raw DNA-PAINT data; H.-Y.W. trained N.E. in conducting experiments; J.A. advised on the data analysis and supervised the project; C. S. and F.V. conceived the study. All authors contributed to writing the manuscript.

Notes

The authors declare no competing financial interests.

ACKNOWLEDGMENT

N.E. acknowledges funding from the EPSRC Centre for Doctoral Training (CDT) in Metamaterials (XM2) at the University of Exeter. N.E., H.-Y.W. and F.V. acknowledge support from EPSRC (EP/R031428/1). S.S., J.R., J.A. and F.V. acknowledge support from EPSRC (EP/T002875/1). J.A. acknowledges support from EPSRC (EP/R045577/1) and the Royal Society. C.S. acknowledges support from EPSRC (EP/N008235/1).

REFERENCES

1. Lenn, T.; Leake, M. C., Experimental approaches for addressing fundamental biological questions in living, functioning cells with single molecule precision. *Open biology* **2012,** *2* (6), 120090.

2. Miller, H.; Zhou, Z.; Shepherd, J.; Wollman, A. J.; Leake, M. C., Single-molecule techniques in biophysics: a review of the progress in methods and applications. *Reports on Progress in Physics* **2017,** *81* (2), 024601.

3. Capitanio, M.; Pavone, F. S., Interrogating biology with force: single molecule high-resolution measurements with optical tweezers. *Biophysical journal* **2013,** *105* (6), 1293-1303.

4. Yu, B.; Chen, D.; Qu, J.; Niu, H., Fast Fourier domain localization algorithm of a single molecule with nanometer precision. *Optics letters* **2011,** *36* (22), 4317-4319.

5. Kufer, S. K.; Strackharn, M.; Stahl, S. W.; Gumpp, H.; Puchner, E. M.; Gaub, H. E., Optically monitoring the mechanical assembly of single molecules. *Nature nanotechnology* **2009,** *4* (1), 45-49.

6. Hinterdorfer, P.; Dufrêne, Y. F., Detection and localization of single molecular recognition events using atomic force microscopy. *Nature methods* **2006,** *3* (5), 347-355.

7. Rust, M. J.; Bates, M.; Zhuang, X., Sub-diffraction-limit imaging by stochastic optical reconstruction microscopy (STORM). *Nature methods* **2006,** *3* (10), 793-796.

8. Betzig, E.; Patterson, G. H.; Sougrat, R.; Lindwasser, O. W.; Olenych, S.; Bonifacino, J. S.; Davidson, M. W.; Lippincott-Schwartz, J.; Hess, H. F., Imaging intracellular fluorescent proteins at nanometer resolution. *Science* **2006,** *313* (5793), 1642-1645.

9. Hess, S. T.; Girirajan, T. P.; Mason, M. D., Ultra-high resolution imaging by fluorescence photoactivation localization microscopy. *Biophysical journal* **2006,** *91* (11), 4258-4272.

10. Jungmann, R.; Avendaño, M. S.; Woehrstein, J. B.; Dai, M.; Shih, W. M.; Yin, P., Multiplexed 3D cellular super-resolution imaging with DNA-PAINT and Exchange-PAINT. *Nature methods* **2014,** *11* (3), 313-318.

11. Schnitzbauer, J.; Strauss, M. T.; Schlichthaerle, T.; Schueder, F.; Jungmann, R., Super-resolution microscopy with DNA-PAINT. *Nature protocols* **2017,** *12* (6), 1198.

12. Lin, R.; Clowsley, A. H.; Lutz, T.; Baddeley, D.; Soeller, C., 3D super-resolution microscopy performance and quantitative analysis assessment using DNA-PAINT and DNA origami test samples. *Methods* **2020,** *174*, 56-71.

13. Sepúlveda, B.; Angelomé, P. C.; Lechuga, L. M.; Liz-Marzán, L. M., LSPR-based nanobiosensors. *nano today* **2009,** *4* (3), 244-251.

14. Zhang, W.; Caldarola, M.; Lu, X.; Pradhan, B.; Orrit, M., Single-molecule fluorescence enhancement of a near-infrared dye by gold nanorods using DNA transient binding. *Physical Chemistry Chemical Physics* **2018,** *20* (31), 20468-20475.

15. Malinsky, M. D.; Kelly, K. L.; Schatz, G. C.; Van Duyne, R. P., Chain length dependence and sensing capabilities of the localized surface plasmon resonance of silver nanoparticles chemically modified with alkanethiol self-assembled monolayers. *Journal of the American Chemical Society* **2001,** *123* (7), 1471-1482.

16. Haes, A. J.; Zou, S.; Schatz, G. C.; Van Duyne, R. P., A nanoscale optical biosensor: the long range distance dependence of the localized surface plasmon resonance of noble metal nanoparticles. *The Journal of Physical Chemistry B* **2004,** *108* (1), 109-116.

17. Nusz, G. J.; Curry, A. C.; Marinakos, S. M.; Wax, A.; Chilkoti, A., Rational selection of gold nanorod geometry for label-free plasmonic biosensors. *ACS nano* **2009,** *3* (4), 795-806.

18. Baaske, M. D.; Foreman, M. R.; Vollmer, F., Single-molecule nucleic acid interactions monitored on a label-free microcavity biosensor platform. *Nature nanotechnology* **2014,** *9* (11), 933.

19. Baaske, M. D.; Vollmer, F., Optical observation of single atomic ions interacting with plasmonic nanorods in aqueous solution. *Nature Photonics* **2016,** *10* (11), 733-739.

20. Vincent, S.; Subramanian, S.; Vollmer, F., Optoplasmonic characterisation of reversible disulfide interactions at single thiol sites in the attomolar regime. *Nature Communications* **2020,** *11* (1), 1-8.

21. Dietz, M. S.; Wehrheim, S. S.; Harwardt, M. I. E.; Niemann, H. H.; Heilemann, M., Competitive Binding Study Revealing the Influence of Fluorophore Labels on Biomolecular Interactions. *Nano Lett* **2019,** *19* (11), 8245-8249.

22. Peterson, E. M.; Reece, E. J.; Li, W.; Harris, J. M., Super-Resolution Imaging of Competitive Unlabeled DNA Hybridization Reveals the Influence of Fluorescent Labels on Duplex Formation and Dissociation Kinetics. *J Phys Chem B* **2019,** *123* (50), 10746-10756.

23. Zimmers, Z. A.; Adams, N. M.; Gabella, W. E.; Haselton, F. R., Fluorophore-Quencher Interactions Effect on Hybridization Characteristics of Complementary Oligonucleotides. *Anal Methods* **2019,** *11* (22), 2862-2867.

24. Willets, K. A., Supercharging superlocalization microscopy: how electrochemical charging of plasmonic nanostructures uncovers hidden heterogeneity. *ACS nano* **2019,** *13* (6), 6145-6150.

25. Byers, C. P.; Hoener, B. S.; Chang, W.-S.; Yorulmaz, M.; Link, S.; Landes, C. F., Single-particle spectroscopy reveals heterogeneity in electrochemical tuning of the localized surface plasmon. *The Journal of Physical Chemistry B* **2014,** *118* (49), 14047-14055.

26. Kaushal, S.; Nanda, S. S.; Yi, D. K.; Ju, H., Effects of Aspect Ratio Heterogeneity of an Assembly of Gold Nanorod on Localized Surface Plasmon Resonance. *The Journal of Physical Chemistry Letters* **2020,** *11* (15), 5972-5979.

27. Taylor, A.; Verhoef, R.; Beuwer, M.; Wang, Y.; Zijlstra, P., All-optical imaging of gold nanoparticle geometry using super-resolution microscopy. *The Journal of Physical Chemistry C* **2018,** *122* (4), 2336-2342.

28. Jungmann, R.; Steinhauer, C.; Scheible, M.; Kuzyk, A.; Tinnefeld, P.; Simmel, F. C., Single-molecule kinetics and super-resolution microscopy by fluorescence imaging of transient binding on DNA origami. *Nano letters* **2010,** *10* (11), 4756-4761.

29. Andrews, R., DNA hybridisation kinetics using single-molecule fluorescence imaging. *Essays in Biochemistry* **2021**.